Journal of Catalysis 257 (2008) 221–228

Contents lists available at ScienceDirect

Journal of Catalysis

www.elsevier.com/locate/jcat

A DFT study of the chain growth probability in Fischer–Tropsch synthesis

Jun Cheng [a], P. Hu [a,*], Peter Ellis [b], Sam French [b], Gordon Kelly [c], C. Martin Lok [c]

[a] School of Chemistry and Chemical Engineering, The Queen's University of Belfast, Belfast, BT9 5AG, UK
[b] Johnson Matthey Technology Centre, Reading, RG4 9NH, UK
[c] Johnson Matthey Technology Centre, Billingham Cleveland, TS23 1LB, UK

ARTICLE INFO

Article history:
Received 27 December 2007
Revised 22 April 2008
Accepted 3 May 2008
Available online 2 June 2008

Keywords:
Fischer–Tropsch
DFT
Co
Chain growth probability
C–C coupling
Methane

ABSTRACT

The chain growth probability (α value) is one of the most significant parameters in Fischer–Tropsch (FT) synthesis. To gain insight into the chain growth probability, we systematically studied the hydrogenation and C–C coupling reactions with different chain lengths on the stepped Co(0001) surface using density functional theory calculations. Our findings elucidate the relationship between the barriers of these elementary reactions and the chain length. Moreover, we derived a general expression of the chain growth probability and investigated the behavior of the α value observed experimentally. The high methane yield results from the lower chain growth rate for $C_1 + C_1$ coupling compared with the other coupling reactions. After C_1, the deviation of product distribution in FT synthesis from the Anderson–Schulz–Flory distribution is due to the chain length-dependent paraffin/olefin ratio.

1. Introduction

Fischer–Tropsch (FT) synthesis [1–8] is a complex catalytic process in which a mixture of CO and H_2 (synthesis gas) is converted to various long-chain hydrocarbons and water over VIII group metals (mainly Fe, Co, and Ru). Its products can be used as feedstock in the chemical industry and transportation fuel market as a substitute for conventional crude oil. Intensive effort has been dedicated to FT synthesis [9–20] since it was discovered about 80 years ago [21], and great progress has been made experimentally [22–24] and theoretically [25,26]. Generally, the intricate process can be described as follows: First, CO and H_2 dissociate on catalyst surfaces, followed by removal of O through water formation and desorption. Meanwhile, surface intermediates, CH_x ($x = 0$–3), are formed from the hydrogenation of C atoms. Then the carbon chains are propagated from the initial chains via stepwise polymerization of the CH_x. Finally, the carbon chains are terminated mainly by β-hydrogen elimination yielding α-olefins or by α-hydrogenation producing n-paraffins.

Because the FT products are a complex mixture of many organic compounds (e.g., paraffins, olefins, oxygenates), the selectivity toward the desired products is the central issue in FT synthesis. One of the most important selectivities is the C_{5+} selectivity. Because ultraclean liquid fuels are of industrial interest, it is crucial to improve the selectivity to C_{5+} and suppress the formation of unwanted methane in FT synthesis. The α value, defined as the probability of chain growth, is a good parameter for evaluating C_{5+} selectivity and is used widely to study FT synthesis [27,28]. As illustrated in Fig. 1, the α value can be expressed as

$$\alpha_n = \frac{r_{g,n}}{r_{g,n} + r_{d,n}}, \tag{1}$$

where n is the chain length, $r_{g,n}$ is the chain growth rate, and $r_{d,n}$ is the chain termination rate. Experimentally, the α value can be obtained from the product distribution.

Because the products are formed via stepwise chain growth reactions, the product yield decreases exponentially with the chain length, following the so-called Anderson–Schulz–Flory (ASF) [29,30] distribution. An ideal ASF distribution can be written as

$$M_n = M_1 \cdot \alpha^{n-1}, \tag{2}$$

where M_n is the molar fraction of products with the chain length n. In this case, the α value is independent of the chain

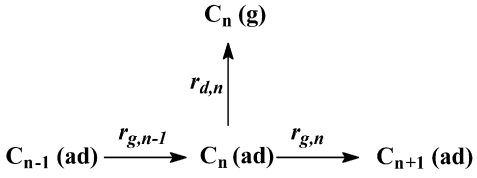

Fig. 1. Scheme of the chain growth and termination of surface species C_n. $r_{g,n-1}$ and $r_{g,n}$ are chain growth rates with chain length $n-1$ and n, respectively, and $r_{d,n}$ is chain termination rate with chain length n.

* Corresponding author. Fax: +44 (0) 28 9097 4687.
E-mail address: p.hu@qub.ac.uk (P. Hu).

0021-9517/$ – see front matter
doi:10.1016/j.jcat.2008.05.006

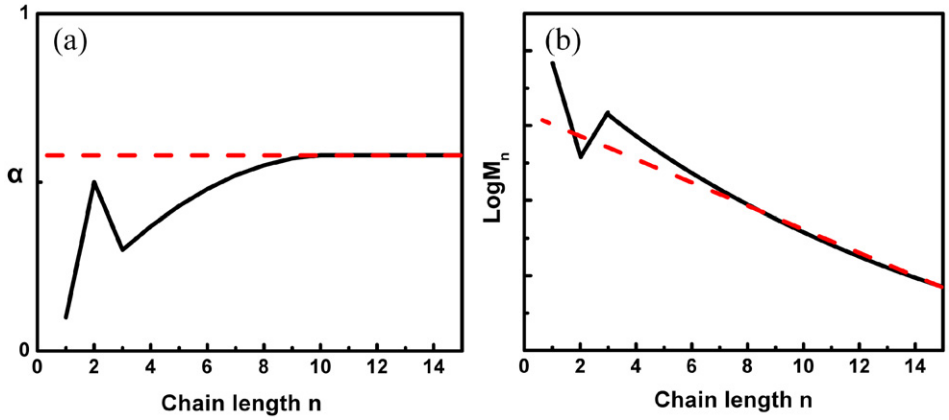

Fig. 2. Illustrative plots of the α value and product molar fraction against the chain length in the cases of the ideal and deviated ASF distribution. The red dashed curves represent the ideal ASF distribution and the black solid curves represent the deviated ASF distribution.

length, and the α value and M_n are represented by the dashed lines in Fig. 2a and 2b, respectively.

Earlier experimental results demonstrated that the α value usually varies with chain length, leading to a deviated ASF distribution [28,30]. As illustrated in Fig. 2a, the α value can be divided into four aspects under typical reaction conditions: (i) When the chain length is very long (i.e., $n > 10$), the α value is almost constant; (ii) the α value decreases with a decrease in chain length from ~10 to 3; (iii) when the chain length is 2, the α value is abnormally high; and (iv) for CH_4, the α value is the smallest. The erratic nature of the α value (Fig. 2a) results in the deviated ASF distribution (Fig. 2b), with a high methane molar fraction, a low C_2 molar fraction, and a curvature after C_2.

Several explanations for the relatively high methane fraction have been advanced in the literature. The most popular explanation is the existence of an extra catalytic site for the methanation reaction, suggested by Schulz et al. [31,32]. But these authors did not specify the exact nature of this site, and did not provide any direct evidence to verify the existence of this site. Other authors proposed that the high yield of methane can be attributed in part to the secondary hydrogenolysis of hydrocarbons [12,27]. However, Schulz et al. [30] reported that their olefin cofeeding studies on the Co catalyst demonstrated no indication of methane formation from hydrogenolytic C–C bond-rupture reactions of higher hydrocarbons. Earlier ^{14}C-labeling work by Koelbel et al. [33] also showed that the amounts of methane formed by catalytic hydrocracking of primarily obtained hydrocarbons account for only a very small percentage of the total methane formed under normal synthesis conditions on Co, Ni, and Fe catalysts. Dry [34] suggested that heat and mass transfer limitations may result in increases of thermodynamically favored products, such as methane, but cannot explain the common observation of high methane yield even in the absence of heat and mass transfer limitations.

Some authors have attributed the deviation of product distribution after C_1 to the presence of several types of active sites with different probabilities for chain growth and for chain termination to form olefins and paraffins, because the deviated ASF distribution often could be fitted by a superposition of two ASF distributions on Fe catalysts [35,36]. However, Iglesia et al. [37–40] found that multisite models alone cannot explain the selectivity changes that occur with increasing chain size, bed residence time, and site density on Ru and Co catalysts. A more plausible cause of the deviation is the chain length-dependent olefin readsorption. However, the cause of this chain length dependence is still under debate. Three explanations have been proposed in the literature: chain length-dependent solubility [41,42], diffusivity [37–40], and physisorption [43]. Our recent theoretical study [44] found that the physical origin of the chain length-dependent olefin readsorption is the chain length dependence of both the van der Waals interaction between adsorbed α-olefins and metal surfaces and the entropy difference between adsorbed and gaseous α-olefins. In particular, the anomaly of C_2 often was attributed to the higher readsorption rate of ethylene compared with that of the other α-olefins [37,42]. Our recent work analyzed this issue thoroughly and identified the cause of the C_2 anomaly as the greater chemisorption energy of ethylene [44].

How to promote C_{5+} selectivity is a fundamental issue in FT synthesis. A deeper understanding of the behavior of the α value can contribute greatly to addressing this problem. With the aim of gaining insight into the α value, we studied the chain growth and chain termination reactions with different chain lengths in FT synthesis on the Co surface using DFT calculations.

In previous work [45,46], we studied the $C_1 + C_1$ coupling reactions on both the flat and stepped Co(0001) surfaces and found that these elementary reactions in FT synthesis in general prefer to occur at the step sites and the coupling of $CH_3 + C$ and $CH_2 + CH_2$ at the step sites is the most likely chain growth mechanism for the $C_1 + C_1$ coupling over the Co surface. In the present work, we report in detail the hydrogenation of the C_2 species and the $C_2 + C_1$ coupling reactions (as well as some of the $C_3 + C_1$ coupling) on the stepped Co(0001) surface to investigate the trends of these processes with different chain lengths. The results allow us to study the chain growth and termination rates with different chain lengths in an effort to explain the behavior of the α value on the Co surface.

The paper is organized as follows. In Section 1, we describe our calculation method. In Section 3 we present the calculation results of the hydrogenation of the C_2 species and the $C_2 + C_1$ coupling reactions on the stepped Co(0001) surface. In Section 4, we analyze the common features, as well as specific features of the hydrogenation and $C + C$ coupling reactions with different chain lengths, to explain the role of chain growth probability in FT synthesis. We summarize our conclusions in Section 5.

2. Methods

In this work, the SIESTA code was used with Troullier–Martins norm-conserving scalar relativistic pseudopotentials [47–49]. A double-zeta plus polarization (DZP) basis set was used. The localization radii of the basis functions were determined from an energy shift of 0.01 eV. A standard DFT supercell approach with the Perdew–Burke–Ernzerhof form of the generalized gradient approximation (GGA) functional was implemented, and the Kohn–Sham orbitals were expanded in a localized basis (double-zeta) set with

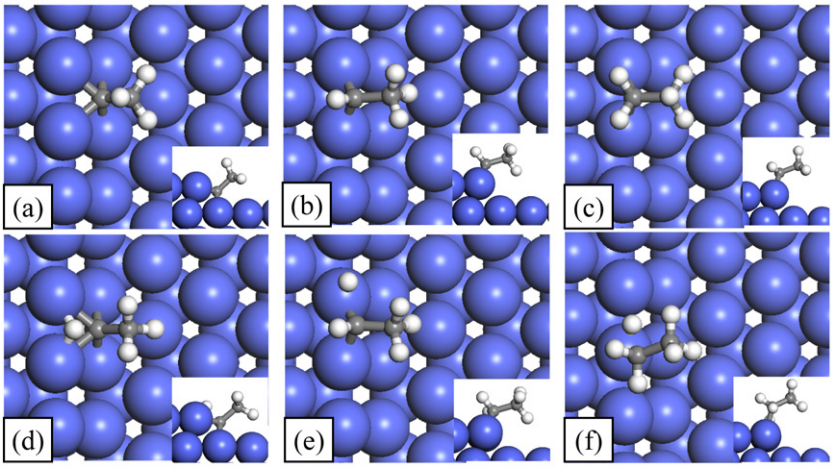

Fig. 3. Top view and side view (inserted) of the ISs (upper row) and TSs (lower row) of hydrogenation of C_2 species on the stepped Co(0001) surface. The blue balls are Co, the small grey ones are C and the small white ones are H. This notation is used throughout this paper. (For interpretation of the references to color in this figure legend, the reader is referred to the web version of this article.)

a mesh cutoff of 200 Ry. Spin polarization was included in the calculations. The accuracy of the setting was verified in our previous work [45].

All the reactions were simulated at steps. A $p(4 \times 2)$ unit cell was used, and the stepped Co(0001) surface was modeled by removing two neighboring rows of Co atoms on the top layer (see [45] for details). Monkhorst Pack meshes of $3 \times 5 \times 1$ k-point sampling in the surface Brillouin zone was used on the stepped surface. To avoid the interaction between the adsorbates in neighbouring unit cells, some reactions at steps (i.e., $CH_3CH + CH_2$ and $CH_3CH_2 + CH_2$) were studied in the $p(4 \times 3)$ unit cell with Monkhorst Pack meshes of $3 \times 4 \times 1$ k-point sampling in the surface Brillouin zone. In the calculations, the surface was modeled by four layers of metals; the bottom two layers of metal atoms were fixed, and the top two layers and the adsorbates were relaxed.

The transition states (TSs) were searched using a constrained optimization scheme [50–52]. The distance between the reactants is constrained at an estimated value, and the total energy of the system is minimized with respect to all other degrees of freedom. The TSs can be located via changing the fixed distance, and must be confirmed by the following two rules: (i) All forces on atoms vanish, and (ii) the total energy is maximum along the reaction coordinate but minimum with respect to the remaining degrees of freedom.

3. Results

3.1. Hydrogenation of the C_2 species

Our group recently studied the hydrogenation reactions of all of the C_1 species (C, CH, CH_2, and CH_3) on the stepped Co(0001) surface and found that the step-corner sites were favored for C and CH, whereas the edge-bridge sites were favored for CH_2 and CH_3 [53]. In the present work, we found that the adsorbed C_2 species (initial states [ISs]) have similar geometries to their C_1 counterparts [Fig. 3a–3c]. We also located the TSs of hydrogenation of C_2 species on the stepped Co(0001) surface. As shown in Fig. 3d–3f, the geometries of TSs also were very similar to those of C_1 species [45,53].

The barriers and structural parameters at the TSs of the hydrogenation of C_2 species are given in Table 1. As the table shows, the results for the C_2 species also were very similar to those of the C_1 species [45,53]. For example, in the case of RC (R = H or CH_3) hydrogenation, the barrier and the distance between the reacting C and H were 0.80 eV and 1.44 Å, respectively, for the CH + H reaction compared with 0.86 eV and 1.38 Å for the CH_3C + H reaction.

Table 1
Barriers and distances between the reacting C and H at the TSs of hydrogenation of C_2 species on the stepped Co(0001) surface

	$CH_3C + H$	$CH_3CH + H$	$CH_3CH_2 + H$
Barrier (eV)	0.86	0.42	0.82
Distance (Å)	1.38	1.72	1.59

3.2. The $C_2 + C_1$ coupling reactions

Based on the TS structures of $C_1 + C_1$ coupling reactions reported in our previous work [45], we further located the TSs of the $C_2 + C_1$ coupling. In our calculations, we considered only CH_3C (CH-like), CH_3CH (CH_2-like), and CH_3CH_2(CH_3-like) as the growing chains and C, CH, and CH_2 as the monomers. The other C_2 species, such as CHCH and CH_2C, which contain two unsaturated C atoms, are not likely to be the growing chains, for several reasons:

1. Those C_2 species bind the metal surface with two unsaturated C atoms and occupy more surface sites than CH_3C, CH_3CH, and CH_3CH_2 (upright structures). Considering that the surface coverage is generally very high under FT reaction conditions, the C_2 species with one saturated C atom are thermodynamically unfavored compared with the C_2 species with two unsaturated C atoms.
2. The C_3 products of those coupling reactions, binding the surface with three unsaturated C atoms, could be unstable due to the bonding competition (caused by adsorbates sharing bonding with surface atoms) [54,55].
3. Once the C_3 species with three unsaturated C atoms were formed, sequential chain propagation would readily lead to branched carbon chains. But linear hydrocarbons often are the main FT products, whereas the amount of branched products is much smaller.

The coupling reactions with CH_3 as monomer also are excluded, considering that CH_3 is quite repulsive to the growing chain, leading to high barriers. Our previous work [45] also demonstrated that none of the $C_1 + C_1$ couplings involving CH_3 are important to chain growth, except the CH_3 + C coupling, in which the C atom is the monomer and CH_3 is only the growing chain.

Figs. 4a–4i illustrate the calculated structures of the TSs of the $C_2 + C_1$ coupling reactions. Generally, these structures are very sim-

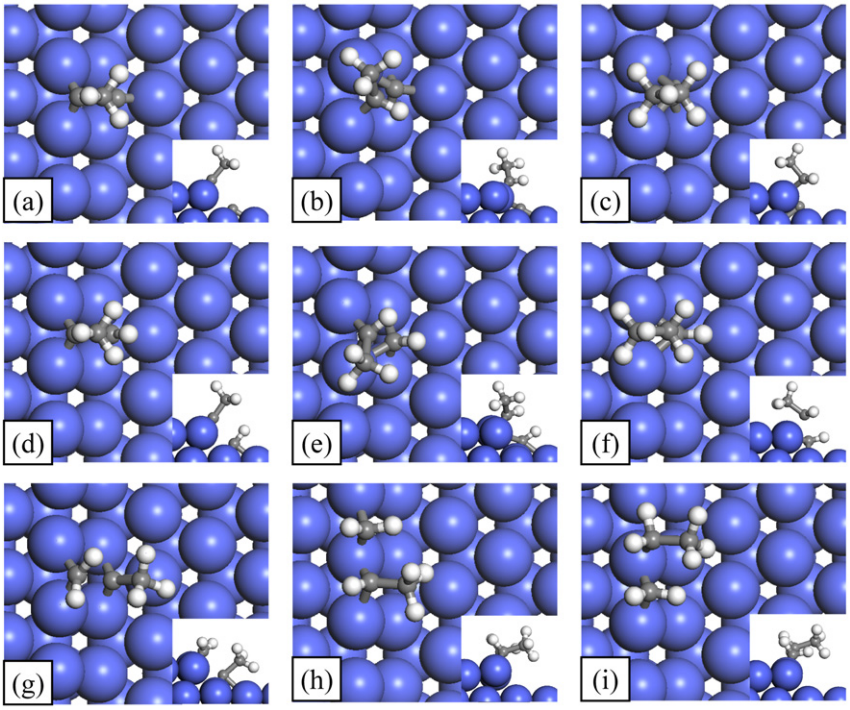

Fig. 4. Top view and side view (inserted) of the TSs of the $C_2 + C_1$ coupling reactions on the stepped Co(0001) surface. (a) $CH_3C + C$; (b) $CH_3CH + C$; (c) $CH_3CH_2 + C$; (d) $CH_3C + CH$; (e) $CH_3CH + CH$; (f) $CH_3CH_2 + CH$; (g) $CH_3C + CH_2$; (h) $CH_3CH + CH_2$; (i) $CH_3CH_2 + CH_2$.

ilar to those of the $C_1 + C_1$ coupling [45]; they can be obtained by replacing the appropriate H with CH_3 at the TSs of the corresponding C_1 counterparts. The C atom is always located on the step-corner site (Fig. 4c) or the 3-fold hollow site on the lower terrace (Fig. 4a and 4b). Similar to the C atom, the CH-like species (CH and CH_3C) usually are found on the step-corner site (Fig. 4f) or the 3-fold hollow site on the lower terrace (Figs. 4d, 4e and 4g); however, when they react with C and CH, they move to the step-edge site Figs. 4a and 4d at the TSs. The CH_2-like and CH_3-like species are always near the step-edge site as both the monomer and the growing chain. In general, these TS structures are in line with the rule proposed by Michaelides and Hu for predicting the TSs of chemical reactions on catalyst surfaces [56]: The higher valency of the adsorbate, the greater its tendency to access a TS close to a high coordination site.

The calculated barriers and structural parameters of the coupling reactions are listed in Table 2. Based on the barriers of the $C_2 + C_1$ coupling and the $C_1 + C_1$ coupling [45], these coupling reactions can be divided into three classes: I, II, and III.

Class I comprises the coupling reactions of $CH_3CH + C$, $CH_3CH_2 + C$, $CH_3CH + CH$, $CH_3CH + CH_2$, and $CH_3CH_2 + CH_2$, in which the barriers are very similar to those of the corresponding $C_1 + C_1$ coupling. In particular, $RCH_2 + C$ and $RCH + CH_2$, the most likely chain growth pathways that we identified in previous work [45], belong to this class. When R = H, the barriers of $RCH_2 + C$ and $RCH + CH_2$ are 1.09 eV and 0.22 eV, respectively, very similar to the 1.18 eV and 0.29 eV seen when $R = CH_3$.

Class II contains the coupling reactions of $CH_3C + CH_2$ and $CH_3CH_2 + CH$, in which the barriers are greater than those of the corresponding $C_1 + C_1$ coupling. For example, the coupling barrier of $CH_3C + CH_2$ (1.61 eV) is 0.29 eV higher than that of $CH + CH_2$ (1.32 eV).

The coupling reactions of $CH_3C + C$ and $CH_3C + CH$ belong to class III, in which the barriers are smaller than those of the corresponding $C_1 + C_1$ coupling. For instance, the coupling barrier of $CH_3C + C$ (1.58 eV) is 0.38 eV smaller than that of $CH + C$ (1.96 eV). We analyze these further in Section 4.

Table 2
Barriers and distances between the two reacting C atoms at the TSs of the $C_2 + C_1$ coupling reactions on the stepped Co(0001) surface

Pathway	$CH_3C + C$	$CH_3CH + C$	$CH_3CH_2 + C$
Barrier (eV)	1.58	1.28	1.18
Distance (Å)	2.63	2.18	2.02
Pathway	$CH_3C + CH$	$CH_3CH + CH$	$CH_3CH_2 + CH$
Barrier (eV)	1.44	1.41	1.75
Distance (Å)	2.26	2.12	1.90
Pathway	$CH_3C + CH_2$	$CH_3CH + CH_2$	$CH_3CH_2 + CH_2$
Barrier (eV)	1.61	0.29	0.74
Distance (Å)	2.21	2.13	2.10

4. Discussion

4.1. Hydrogenation of the surface species with different chain lengths

As noted in Section 3.1, the structural similarities of the ISs and TSs of the hydrogenation of the C_1 and C_2 species give rise to similar barriers for these processes on the stepped Co(0001) surface. The energy profiles of these hydrogenation reactions of the C_1 and C_2 species, shown in Fig. 5, clearly reveal that both energy profiles are similar, although there is a small difference (around 0.1 eV) in the energy levels of ISs and TSs of the hydrogenation step of $CH_2(RCH) + H$. Because the changes in the ISs and TSs of the hydrogenation reactions are effectively a replacement of H by CH_3 when the chain length increases by 1, we would expect that the structural similarity could be extended to longer chain lengths. This means that energy profiles for all other chain lengths are similar to that shown in Fig. 5.

Recently, our DFT calculations showed that CH_3 hydrogenation is the slowest step in the sequence of C hydrogenation on flat and stepped Co surfaces [45], which is consistent with experimental work [38,57]. Thus, the preceding hydrogenation steps may reach quasi-equilibrium. Consequently, the coverages of the C_1 species

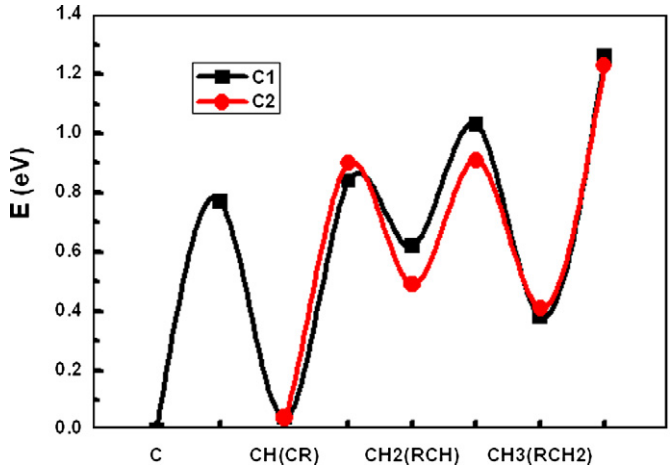

Fig. 5. Energy profiles of the C_1 and C_2 hydrogenation reactions on the stepped Co(0001) surface. The energy profile in black is for C_1 species and the one in red is for C_2 species. R is an alkyl group (i.e. CH_3 for C_2 species). The energy level of C atom is chosen as the zero point. The energy profile of C_2 species is arranged in the graph by aligning the energy level of CH_3C with that of CH.

(θ_{CH_i}) can be expressed with reference to the C coverage (θ_C) at step sites:

$$\theta_{CH_i} = e^{-E_i/RT}\theta_C t^i, \quad i = 0, 1, 2, 3, \tag{3}$$

where t is the ratio of H coverage to free surface site coverage (θ_H/θ_*), which is around 1 under typical reaction conditions [45], and E_i is the energy difference between adsorbed CH_i and C.

Because the hydrogenation reactions of the surface species with longer chain lengths have a similar energy profile as the C_1 species, these reactions also may reach quasi-equilibrium under steady-state conditions. Their coverages (θ_{RCH_j}) can be expressed in a similar way as in Eq. (3) as follows:

$$\theta_{RCH_j} = e^{-E'_j/RT}\theta_{RC} t^j, \quad j = 0, 1, 2, \tag{4}$$

where the coverage (θ_{RC}) of the CH-like species (RC) is a reference, R is an alkyl group, and E'_j is the energy difference between adsorbed RCH_j and RC, which is independent of chain length.

4.2. C–C coupling reactions of the growing chains with different chain lengths

In Section 3.2, we showed that the geometries of the TSs of the $C_2 + C_1$ coupling reactions are very similar to those of the $C_1 + C_1$ coupling reactions. This is true for the hydrogenation reactions as well. However, the barriers of hydrogenation reactions of the C_1 species are similar to those of the C_2 species, whereas the barriers of some $C_2 + C_1$ coupling reactions differ greatly from those of the corresponding $C_1 + C_1$ coupling reactions; for example, the barrier difference between the coupling of $CH_3C + C$ and that of $CH + C$ is as large as 0.4 eV. As noted in Section 3.2, the C–C coupling reactions are divided into three classes based on their barriers.

To understand our calculation results, we used the barrier decomposition scheme [58–60] to analyze the reaction barriers quantitatively. The decomposition procedure of the A + B coupling is illustrated in Fig. 6, and the coupling barrier can be expressed as

$$E_a = \Delta E_A^{TS} + \Delta E_B^{TS} + E_{int}^{TS}, \tag{5}$$

where ΔE_A^{TS} (ΔE_B^{TS}) is the energy cost for reactant A (B) moving from the position at the IS to that at the TS in the absence of reactant B (A), and E_{int}^{TS} is a quantitative measure of the interaction between A and B at the TS.

We applied the barrier decomposition scheme to the four types of the C–C coupling reactions (RC + C, RC + CH, RC + CH_2, and

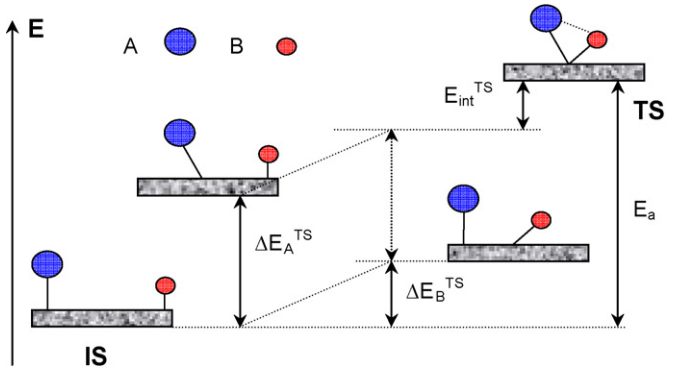

Fig. 6. Energy diagram of the barrier decomposition of the A + B coupling reaction on metal surfaces.

Table 3
Barrier decomposition of the A + B coupling reactions. A is the growing chain, and B is the monomer

A + B	A	B	ΔE_A^{TS}	ΔE_B^{TS}	E_{int}^{TS}	E_a
RC + C	CH	C	**1.10**	0.85	0.01	1.96
	CH_3C	C	**0.73**	0.82	0.03	1.58
RC + CH	CH	CH	**1.07**	0.56	0.13	1.76
	CH_3C	CH	**0.69**	0.53	0.22	1.44
RC + CH_2	CH	CH_2	0.55	0.48	0.29	1.32
	CH_3C	CH_2	0.69	0.46	0.36	1.61
RCH_2 + CH	CH_3	CH	0.48	0.32	0.75	1.55
	CH_3CH_2	CH	0.69	0.38	0.68	1.75

RCH_2 + CH), in which the barriers of the $C_2 + C_1$ coupling differ from those of the corresponding $C_1 + C_1$ coupling. The calculated results, given in Table 3, show that ΔE_B^{TS} (where B is the monomer) of the $C_2 + C_1$ coupling are almost the same as for the corresponding the $C_1 + C_1$ coupling in all the four types of the coupling reactions. This is not surprising, because all of the positions of the monomers (B) are similar in both cases. The interaction term, E_{int}^{TS}, also hardly changes; the greatest change is only 0.09 eV in the case of the RC + CH coupling. However, ΔE_A^{TS} (where A is the growing chain) vary considerably from the $C_1 + C_1$ coupling to the corresponding $C_2 + C_1$ coupling.

Thus, as can be seen from Table 3, the trend of the coupling barrier is determined by ΔE_A^{TS}. This means that from the $C_1 + C_1$ coupling to the corresponding $C_2 + C_1$ coupling, the replacement of H with CH_3 changes the energy costs for the growing chains to move from the positions at the ISs to those at the TSs, leading to different barriers. To investigate these changes, we examined the TS structures of these C–C coupling reactions and found the following.

First, in the case of RCH_2 + CH and RC + CH_2 (Figs. 4f and 4g), there is considerable steric repulsion between C_2 and C_1 due to the extra CH_3 group when C_2 species are close to C_1 to achieve the TSs, whereas the repulsion is much smaller for the corresponding $C_1 + C_1$ coupling. The growing chains (CH_3C and CH_3CH_2) are forced to change to the unfavored geometries, leading to larger ΔE_A^{TS} while E_{int}^{TS} remains unchanged.

Second, in most of the C–C coupling reactions, such large steric repulsions do not occur. In these cases, the extra CH_3 groups are accommodated in the growing chains in a direction that does not cause considerable repulsions. This is why the coupling reactions of $CH_3CH + C$, $CH_3CH_2 + C$, $CH_3CH + CH$, $CH_3CH + CH_2$, and $CH_3CH_2 + CH_2$ have similar barriers to the corresponding $C_1 + C_1$ coupling (see Section 3.2).

Third, for the coupling of $CH_3C + C$ and $CH_3C + CH$, the presence of CH_3 does not increase the barrier but, surprisingly, does

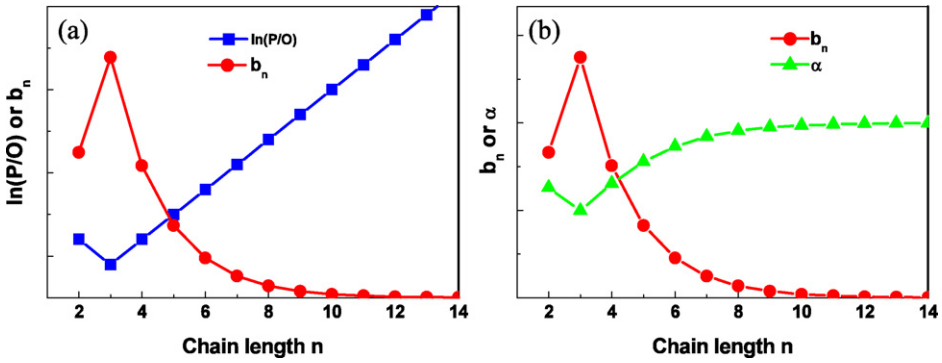

Fig. 7. Illustrative plots of ln(P/O) and b_n and α against the chain length n.

decrease ΔE_A^{TS} (in bold in Table 3) and E_a. In both cases, the growing chain CH_3C moves from the step-corner site at the ISs (Fig. 3a) to the edge-bridge site at the TSs (Figs. 4a and 4d). The energy costs due to the position changes of CH_3C (ΔE_A^{TS}) are 0.37 eV for CH_3C+C and 0.38 eV for CH_3C+CH, smaller than those of the corresponding C_1 species (CH). We note that in these two reactions, the C–C distance in CH_3C decreases from 1.54 Å at the ISs to 1.50 Å at the TSs. This finding is consistent with chemical intuition; when CH_3C sits on the step-corner site, the bonding between C and the four Co atoms is very strong, which weakens the C–C bond in the adsorbate, whereas when CH_3C moves to the edge-bridge site at the TSs, the bonding between C and the metal surface is weakened to release some bonding capability of C to strengthen the C–C bond in CH_3C. But this mechanism is not likely to operate in the cases of the coupling of $CH+C$ and $CH+CH$, because H, unlike CH_3, has a limited bonding capability. This argument may not be applied to the CH_3C+CH_2 coupling (Fig. 4g) involving CH_3C, because the position of CH_3C at the TS is not far from that at the IS.

According to the foregoing analyses, the barriers of the C–C coupling reactions would be expected to not vary when the chain length $n \geqslant 2$. To verify this expectation, we also located the TSs of the coupling of CH_3CH_2C+C and CH_3CH_2C+CH and calculated their barriers (1.63 and 1.47 eV, respectively), which are very close to those of the coupling of CH_3C+C and CH_3C+CH (1.58 and 1.44 eV, respectively).

4.3. Chain growth probability with different chain lengths

In the previous sections, we presented our understanding of the hydrogenation and C–C coupling reactions with different chain lengths. Now we are in a position to investigate the behavior of the chain growth probability with different chain lengths.

The first step toward gaining a better understanding of the chain growth probability is to calculate the chain growth rate. From Eqs. (3) and (4), the chain growth rate ($r_{g,n}$), the sum of the rates of all the C–C coupling pathways, can be expressed as

$$r_{g,n} = \sum_{i,j} r_{RCH_j+CH_i} = \sum_{i,j} Ae^{-E_{i,j}/RT}\theta_{RCH_j}\theta_{CH_i} = \sum_{i,j} Ae^{-(E_{i,j}+E_i+E'_j)/RT}t^{i+j}\theta_{RC}\theta_C, \quad (6)$$

where RC is CH-like species ($CH_3(CH_2)_{n-2}C$), A is the preexponential factor, and $E_{i,j}$ is the barrier of the CH_i+RCH_j coupling reaction. It is noteworthy that the surface coverage of monomer (CH_i) is referenced to C, whereas the surface coverage of growing chain (RCH_j) is referenced to CH-like species (RC). E_i and E'_j are the measures of the relative stabilities of the monomer and growing chain with respect to their respective references (see Section 4.1).

The other aspect of chain growth probability is the chain termination rate. Considering only the major products (linear paraffins and α-olefins) and neglecting the other minor products, which are of very low quantity on Co surface in FT synthesis [8], the chain termination rate, $r_{d,n}$, can be obtained:

$$r_{d,n} = r_{p,n} + r_{o,n}, \quad (7)$$

where $r_{p,n}$ and $r_{o,n}$ are the rates of paraffin and olefin formation, respectively.

Because the hydrogenation reaction of RCH_2+H is irreversible under reaction conditions [57], we can omit the reverse reaction. From Eq. (4), the paraffin formation rate can be written as

$$r_{p,n} = r_{RCH_2+H} = Ae^{-E_a^{hy}/RT}\theta_{RCH_2}\theta_H = Ae^{-(E_a^{hy}+E'_2)/RT}t^2\theta_{RC}\theta_H, \quad (8)$$

where E_a^{hy} is the barrier of the RCH_2+H reaction, which is constant for all of the chain lengths, and E'_2 is the energy difference between RCH_2 and RC.

On the other hand, it is well known [37–41,43,44] that the paraffin/olefin ratio is related to the chain length. Experimental work [61] and also our recent work [44] showed that

$$r_{o,n} = b_n \cdot r_{p,n}, \quad (9)$$

where b_n is an exponential function of the chain length n ($b_n \propto e^{c\cdot n}$, c is a negative) if $n > 2$. We return to this later. Thus, the olefin formation rate can be obtained from the paraffin formation rate.

According to Eqs. (6)–(9), we can obtain the chain growth probability as

$$\alpha_n = \frac{r_{g,n}}{r_{g,n}+r_{d,n}} = \frac{\sum_{i,j} e^{-(E_{i,j}+E_i+E'_j)/RT}t^{i+j}\theta_C}{\sum_{i,j} e^{-(E_{i,j}+E_i+E'_j)/RT}t^{i+j}\theta_C + (1+b_n)\cdot e^{-(E_a^{hy}+E'_2)/RT}t^2\theta_H}, \quad (10)$$

where the preexponential factors and the surface coverage of RC in the numerator and denominator are cancelled. It should be mentioned that the preexponential factor may vary with different chemical reactions, but the difference is usually small for surface reactions.

4.3.1. Chain growth probability when the chain length $n > 1$

As mentioned earlier, both experimental [43,61] and theoretical work [44] has shown that if the chain length $n > 2$, then the logarithm of the paraffin/olefin ratio (ln(P/O)) increases almost linearly with the chain length (the blue curve in Fig. 7a). Thus, b_n decreases exponentially with the chain length n if $n > 2$, as shown by the red curve in Fig. 7a. For the chain length $n = 2$, the paraffin/olefin ratio

is clearly off the line, as shown in the blue curve in Fig. 7a, resulting from the stronger chemisorption energy of ethylene [44]. As a result, b_2 is smaller than the point along the exponential decay curve (the red curve in Fig. 7a).

When the chain length $n > 1$, all the parameters ($E_{i,j}$, E_i, E'_j, $E_{p,d}$, t, θ_C and θ_H) except b_n in Eq. (10) are independent of the chain length under the same reaction conditions. Consequently, the α value is merely affected by b_n for different chain lengths. The relationship between α and b_n is shown in Fig. 7b according to Eq. (10). As can be seen, the anomaly of α for $n = 2$ is due to the smaller b_2, which results from the stronger chemisorption energy of ethylene. For $n > 2$, the α value increases with the chain length because b_n decreases. For long-chain products, b_n is so small that it can be omitted; in other words, the α values of the long chain products can be considered constant, leading to a flat curve after $n > 10$ (the α curve in Fig. 7b).

As can be seen, the chain length-dependent paraffin/olefin ratio results from the chain length-dependent olefin readsorption rate. Thus, our results show that the deviation of the α value after C_1 is indeed due to the chain length-dependent olefin readsorption, which is in line with results reported previously [27,30,37].

It should be mentioned that in the present work we focused on the chain length-dependent behavior of chain growth probability, and the plots in Fig. 7 illustrate the relationship between chain growth probability and chain length. In fact, in addition to the energy terms obtained from the DFT calculations in Eq. (10), we also need the values of t, b_n, θ_C, and θ_H to determine the exact values of chain growth probability, which requires full kinetic consideration that is beyond the scope of the current work.

4.3.2. Chain growth probability when the chain length $n = 1$

The high methane yield has not been satisfactorily explained in the literature. In this section, we explore why methane has the lowest chain growth probability. If the $C_n + C_1$ coupling barriers for $n = 1$ were the same as those for the other chain lengths, then, as can be seen from Eq. (10), the α value for $n = 1$ would be similar to those of the long-chain species, because there is no olefin product for $n = 1$ ($b_1 = 0$). But this is not the case. As discussed in Section 4.2, the coupling barriers of RC + C, RC + CH, RC + CH_2 and RCH_2 + CH for $n = 1$ (i.e., R = H) differ from those for the other chain lengths; this difference affects the chain growth probability.

To semiquantitatively investigate the difference between $n = 1$ and $n \geqslant 2$, we calculated the C–C coupling rates according to Eq. (6). The setting was the same as in our recent work [45]; the temperature was 500 K, and the preexponential factor was 10^{13} s^{-1}, which has proven to be a viable assumption [62–64]. The results are given in Table 4, along with the combined energy terms ($E_{i,j} + E_i + E'_j$), which determine the C–C coupling rates to a great extent. The ratio of H coverage to free site coverage (t) is around 1 and can be omitted [45]. Most of the combined energy terms of the coupling pathways are not altered with different chain lengths, even though there are minor changes in RCH + C and RCH_2 + C (0.19 and 0.13 eV, respectively). For RCH_2 + CH and RC + CH_2, the combined energy terms ($E_{i,j} + E_i + E'_j$) increase from $n = 1$ to $n \geqslant 2$, because the coupling barriers of these two coupling reactions increase, leading to even smaller reaction rates. Most importantly, because the coupling barriers decrease considerably from $n = 1$ to $n \geqslant 2$ for the coupling of RC + C and RC + CH, the combined energy terms ($E_{i,j} + E_i + E'_j$) for $n \geqslant 2$ are so small that these two coupling pathways may make a considerable contribution to the total chain growth rate. Table 4 shows that the reaction rates of these two coupling pathways are comparable to those of RCH_2 + C and RCH + CH_2, the most significant chain growth pathways for $n = 1$ [45]. Therefore, for $n \geqslant 2$, four key chain growth pathways exist: RC + C, RC + CH, RCH_2 + C, and RCH + CH_2. For $n = 1$, only the latter two coupling pathways are important.

Table 4
The energy terms ($E_{i,j} + E_i + E'_j$) and calculated reaction rates of the C–C coupling pathways. n is chain length. The temperature is chosen as 500 K under typical FT reaction conditions in calculating the reaction rates

C–C coupling pathway	RC + C	RCH + C	RCH_2 + C
$n = 1$ $E_{i,j} + E_i + E'_j$ (eV)	**1.96**	1.93	1.43
$r_{RCH_j+CH_i}$ (s^{-1})	$\mathbf{1.7 \times 10^{-7} \theta_{CH} \theta_C}$	$3.5 \times 10^{-7} t \theta_{CH} \theta_C$	$3.8 \times 10^{-2} t^2 \theta_{CH} \theta_C$
$n \geqslant 2$ $E_{i,j} + E_i + E'_j$ (eV)	**1.58**	1.74	1.56
$r_{RCH_j+CH_i}$ (s^{-1})	$\mathbf{1.2 \times 10^{-3} \theta_{RC} \theta_C}$	$2.9 \times 10^{-5} t \theta_{RC} \theta_C$	$1.9 \times 10^{-3} t^2 \theta_{RC} \theta_C$
C–C coupling pathway	**RC + CH**	**RCH + CH**	**RCH_2 + CH**
$n = 1$ $E_{i,j} + E_i + E'_j$ (eV)	**1.8**	1.94	1.94
$r_{RCH_j+CH_i}$ (s^{-1})	$\mathbf{7.1 \times 10^{-6} t \theta_{CH} \theta_C}$	$2.8 \times 10^{-7} t^2 \theta_{CH} \theta_C$	$2.8 \times 10^{-7} t^3 \theta_{CH} \theta_C$
$n \geqslant 2$ $E_{i,j} + E_i + E'_j$ (eV)	**1.48**	1.91	2.17
$r_{RCH_j+CH_i}$ (s^{-1})	$\mathbf{1.2 \times 10^{-2} t \theta_{RC} \theta_C}$	$5.5 \times 10^{-7} t^2 \theta_{RC} \theta_C$	$1.3 \times 10^{-9} t^3 \theta_{RC} \theta_C$
C–C coupling pathway	**RC + CH_2**	**RCH + CH_2**	**RCH_2 + CH_2**
$n = 1$ $E_{i,j} + E_i + E'_j$ (eV)	1.94	1.42	1.69
$r_{RCH_j+CH_i}$ (s^{-1})	$2.8 \times 10^{-7} t^2 \theta_{CH} \theta_C$	$4.8 \times 10^{-2} t^3 \theta_{CH} \theta_C$	$9.2 \times 10^{-5} t^4 \theta_{CH} \theta_C$
$n \geqslant 2$ $E_{i,j} + E_i + E'_j$ (eV)	2.22	1.37	1.74
$r_{RCH_j+CH_i}$ (s^{-1})	$4.2 \times 10^{-10} t^2 \theta_{RC} \theta_C$	$1.5 \times 10^{-1} t^3 \theta_{RC} \theta_C$	$2.9 \times 10^{-5} t^4 \theta_{RC} \theta_C$

According to the foregoing analyses, the chain growth rate for $n \geqslant 2$ may be much larger than that for $n = 1$. On the other hand, their paraffin formation rates are very similar. Thus, the chain growth probability for $n = 1$ is smaller than that for $n \geqslant 2$.

4.3.3. General discussion

Equation (10) is a general expression of the chain growth probability. This equation provides some clues on ways to improve the α value and C_{5+} selectivity. First, increasing θ_C or decreasing θ_H can improve the α value. An increase of the CO partial pressure in the system can facilitate CO dissociation on Co catalysts, resulting in an increase of θ_C and a decrease of θ_H. This can be used to explain the experimental finding [65]; increasing the total pressure will enhance the value of α and suppress methane formation on Co catalysts. The addition of small amounts of water was also found to accelerate CO dissociation [66]. By this means, θ_C is increased to suppress methane formation and improve C_{5+} selectivity. Second, a decrease in olefin formation will reduce the olefin/paraffin ratio (b_n), also leading to a higher α value. This finding is in agreement with many previous experimental results [27,37,38]. The readsorption of α-olefin reverses the termination of β-dehydrogenation, causing an increase in the chain growth probability.

5. Conclusion

Our extensive DFT calculations and detailed analyses have provided deeper insight into the chain growth probability in FT synthesis. Based on our findings, we can draw the following conclusions:

1. The ISs and the TSs of the hydrogenation reactions with different chain lengths have similar geometries. The hydrogenation processes with different chain lengths (RC + 3H → RCH + 2H → RCH_2 + H → RCH_3) also have similar energy profiles.
2. The barriers of all of the $C_n + C_1$ coupling reactions are independent of chain length when the chain length $n > 1$. However, there are some differences between $n \geqslant 2$ and $n = 1$ in the $C_n + C_1$ coupling reactions. Most of the $C_n + C_1$ ($n \geqslant 2$) coupling reactions (RCH + C, RCH_2 + C, RCH + CH, RCH + CH_2, and RCH_2 + CH_2) still have similar barriers to the corresponding $C_1 + C_1$ coupling reactions; however, the RC + CH_2 and RCH_2 + CH coupling reactions have higher barriers than the corresponding $C_1 + C_1$ coupling reactions, due to steric repulsions at the TSs, whereas the RC + C and RC + CH coupling reactions have lower barriers due to the lower energy costs of the growing chain (RC) moving from the ISs to the TSs.

3. We derived a general expression of the chain growth probability [Eq. (10)]. Based on this equation, the behavior of the chain growth probability for $n > 1$ is attributed to the chain-length dependence of the paraffin/olefin formation rate. The smallest chain growth probability for $n = 1$ results from the smaller number of the major $C_n + C_1$ coupling pathways for $n = 1$ (2 pathways) compared with those for $n \geqslant 2$ (4 pathways).

Acknowledgments

The authors thank the Queen's University of Belfast for computing time. J.C. acknowledges Johnson Matthey for financial support.

References

[1] M.E. Dry, Appl. Catal. A 138 (1996) 319.
[2] M.E. Dry, Catal. Today 71 (2002) 227.
[3] H. Schulz, Appl. Catal. A 186 (1999) 3.
[4] J.J.C. Geerlings, J.H. Wilson, G.J. Kramer, H.P.C.E. Kuipers, A. Hoek, H.M. Huisman, Appl. Catal. A 186 (1999) 27.
[5] P. Biloen, W.M.H. Sachtler, Adv. Catal. 30 (1981) 165.
[6] C.K. Rofer-Depoorter, Chem. Rev. 81 (1981) 447.
[7] E. Iglesia, Appl. Catal. A 161 (1997) 59.
[8] B. Jager, R. Espinoza, Catal. Today 23 (1995) 17.
[9] R.A. Dictor, A.T. Bell, J. Catal. 97 (1986) 121.
[10] J.G. Ekerdt, A.T. Bell, J. Catal. 62 (1980) 19.
[11] K.R. Krishna, A.T. Bell, J. Catal. 139 (1993) 104.
[12] T. Komaya, A.T. Bell, J. Catal. 146 (1994) 237.
[13] P.M. Maitlis, R. Quyoum, H.C. Long, M.L. Turner, Appl. Catal. A 186 (1999) 363.
[14] M.L. Turner, P.K. Byers, H.C. Long, P.M. Maitlis, J. Am. Chem. Soc. 115 (1993) 4417.
[15] M.L. Tuner, N. Marsih, B.E. Man, R. Quyoum, H.C. Long, P.M. Maitlis, J. Am. Chem. Soc. 124 (2002) 10456.
[16] (a) H.H. Scorch, N. Goulombic, R.B. Anderson, The Fischer–Tropsch and Related Syntheses, Wiley, New York, 1951;
(b) J.F. Kummer, P.H. Emmett, J. Am. Chem. Soc. 75 (1953) 5177.
[17] H. Pichler, H. Schulz, Chem. Ing. Tech. 12 (1970) 1160.
[18] W.A.A. van Barneveld, V. Ponec, J. Catal. 88 (1984) 382.
[19] I.M. Ciobîcă, F. Frechard, R.A. van Santen, A.W. Kleyn, J. Hafner, Chem. Phys. Lett. 311 (1999) 185.
[20] I.M. Ciobîcă, Ph.D. thesis, Eindhoven University of Technology, Eindhoven, Netherlands, 2002.
[21] F. Fischer, H. Tropsch, Brennstoff Chem. 4 (1923) 276;
F. Fischer, H. Tropsch, Brennstoff Chem. 7 (1926) 79;
F. Fischer, H. Tropsch, Chem. Ber. 59 (1926) 830.
[22] R. Brady, R. Pettit, J. Am. Chem. Soc. 102 (1980) 6181.
[23] R. Brady, R. Pettit, J. Am. Chem. Soc. 103 (1981) 1287.
[24] J. Wilson, C. de Groot, J. Phys. Chem. 99 (1995) 7860.
[25] Z.-P. Liu, P. Hu, J. Am. Chem. Soc. 124 (2002) 11568.
[26] I.M. Ciobîcă, G.J. Kramer, Q. Ge, M. Neurock, R.A. van Santen, J. Catal. 212 (2002) 136.
[27] E.W. Kuipers, C. Scheper, J.H. Wilson, I.H. Vinkenburg, H. Oosterbeek, J. Catal. 158 (1996) 288.
[28] H. Schulz, Top. Catal. 26 (2003) 1.
[29] R.A. Friedel, R.B. Anderson, J. Am. Chem. Soc. 72 (1950) 1212, 2307.
[30] H. Schulz, M. Claeys, Appl. Catal. A 186 (1999) 91.
[31] H. Schulz, E. van Steen, M. Claeys, Stud. Surf. Sci. Catal. 81 (1994) 455.
[32] H. Schulz, E. van Steen, M. Claeys, Top. Catal. 2 (1995) 223.
[33] H. Koelbel, H.-B. Ludwig, H. Hammer, J. Catal. 1 (1962) 156.
[34] M.E. Dry, J. Mol. Catal. 17 (1982) 133.
[35] N.O. Egiebor, W.C. Cooper, Appl. Catal. 14 (1985) 323.
[36] G.A. Huff, C.N. Satterfield, J. Catal. 85 (1984) 370.
[37] E. Iglesia, S.C. Reyes, R.J. Madon, J. Catal. 129 (1991) 238.
[38] R.J. Madon, S.C. Reyes, E. Iglesia, J. Phys. Chem. 4 (1991) 7795.
[39] R.J. Madon, E. Iglesia, J. Catal. 139 (1993) 576.
[40] E. Iglesia, S.C. Reyes, R.J. Madon, S.L. Soled, Adv. Catal. 39 (1993) 221.
[41] L.M. Tau, H.A. Dabbagh, B.H. Davis, Energy Fuels 4 (1990) 94.
[42] H. Schulz, M. Claeys, Appl. Catal. A 186 (1999) 71.
[43] E.W. Kuipers, I.H. Vinkenburg, H. Oosterbeek, J. Catal. 152 (1995) 137.
[44] J. Cheng, T. Song, P. Hu, C.M. Lok, P. Ellis, S. French, J. Catal. 255 (2008) 20.
[45] J. Cheng, X.-Q. Gong, P. Hu, C.M. Lok, P. Ellis, S. French, J. Catal. 254 (2008) 285.
[46] J. Cheng, P. Hu, P. Ellis, S. French, G. Kelly, C.M. Lok, J. Phys. Chem. C 112 (2008) 6082.
[47] J.M. Soler, E. Artacho, J.D. Gale, A. García, J. Junquera, P. Ordejón, D. Sánchez-Portal, J. Phys. Condens. Matter 14 (2002) 2745.
[48] N. Troullier, J.L. Martins, Phys. Rev. B 43 (1991) 1993.
[49] J.P. Perdew, K. Burke, M. Ernzerhof, Phys. Rev. Lett. 77 (1996) 3865.
[50] C.-J. Zhang, P. Hu, J. Am. Chem. Soc. 122 (2000) 2134.
[51] C.-J. Zhang, P. Hu, A. Alavi, J. Am. Chem. Soc. 121 (1999) 7931.
[52] A. Alavi, P. Hu, T. Deutsch, P.L. Silvestrelli, J. Hutter, Phys. Rev. Lett. 80 (1998) 3650.
[53] X.-Q. Gong, R. Raval, P. Hu, J. Chem. Phys. 122 (2005) 024711.
[54] K. Bleakley, P. Hu, J. Am. Chem. Soc. 121 (1999) 7644.
[55] Z.-P. Liu, P. Hu, J. Am. Chem. Soc. 125 (2003) 1958.
[56] A. Michaelides, P. Hu, J. Am. Chem. Soc. 122 (2000) 9866.
[57] J.J.C. Geerlings, M.C. Zonnevylle, C.P.M. de Groot, Surf. Sci. 241 (1991) 302.
[58] Z.-P. Liu, P. Hu, J. Chem. Phys. 114 (2001) 8244.
[59] Z.-P. Liu, P. Hu, J. Am. Chem. Soc. 123 (2001) 12596.
[60] Z.-P. Liu, P. Hu, M.H. Lee, J. Chem. Phys. 119 (2003) 6282.
[61] B. Shi, B.H. Davis, Catal. Today 106 (2005) 129.
[62] V.P. Zhdanov, J. Pavlicek, Z. Knor, Catal. Rev. Sci. Eng. 30 (1988) 501.
[63] M. Boudart, G. Djéga-Mariadassou, in: Kinetics of Heterogeneous Catalytic Reactions, Princeton Univ. Press, Princeton, NJ, 1984.
[64] R.D. Cortright, J.A. Dumesic, Adv. Catal. 46 (2002) 161.
[65] G.L. Bezemer, P.B. Radstake, U. Falke, H. Oosterbeek, H.P.C.E. Kuipers, A.J. van Dillen, K.P. de Jong, J. Catal. 237 (2006) 152.
[66] C.J. Bertole, C.A. Mims, G. Kiss, J. Catal. 210 (2002) 84.